Lettieri, A., Elettore, E., Freddi, F., Latour, M., Rizzano, G. (2021) Performance-based assessment of seismic-resilient steel moment resisting frames equipped with innovative column bases connections. The 9th European Conference on Steel and Composite Structures (Eurosteel 2020), Sheffield, UK, 1–3 September 2021. https://doi.org/10.1002/cepa.1481

Performance-based assessment of seismic-resilient steel moment resisting frames equipped with innovative column base connections

Annarosa Lettieri[1], Elena Elettore[1], Fabio Freddi[2], Massimo Latour[1], Gianvittorio Rizzano[1]

Correspondence

Annarosa Lettieri
PhD Student
Department of Civil Engineering
University of Salerno
Via Giovanni Paolo II
84084 Fisciano (SA)
Email: alettieri@unisa.it

Abstract

Low-damage and self-centring column base connections have been proposed in the last two decades as innovative solutions able to provide the seismic resilience in Moment Resisting Frames (MRFs). Although many works have demonstrated the benefits deriving from the adoption of these systems, only a few research studies investigated the significant parameters influencing their self-centring capability. This paper investigates the influence of the frame layout (*i.e.*, storeys and bays number) on the seismic performance of perimeter MRFs equipped with damage-free self-centring column bases previously studied by the authors. Nine case-study perimeter steel MRFs are designed and modelled in OpenSees. Incremental Dynamic Analyses are performed monitoring both global and storey-level Engineering Demand Parameters, including peak and residual interstorey drifts. Fragility curves are subsequently used to evaluate the self-centring capability of the structures. The present study provides insights on the use of the adopted connections for the residual drift reduction of MRFs and defines the boundaries of the investigated parameters for their application. Results highlight that the self-centring behaviour is particularly sensitive to the number of storeys and tends to reduce with the increasing height of MRFs equipped with the proposed connections.

Keywords

Structural Resilience, Moment Resisting Steel Frames, Self-Centring, Damage-Free Column Bases, Residual Drifts.

1 Introduction

Based on most current codes and guidelines (*e.g.*, [1]-[3]), traditional steel moment resisting frames (MRFs), are designed to experience significant inelastic deformation in case of rare seismic events (*i.e.*, Ultimate Limit State). Such an approach implies extensive damage of structural members, involving high economic losses, and permanent plastic deformation (*e.g.*, residual interstorey drifts) which could impair the building reparability after severe seismic events [4]. To overcome these drawbacks several solutions for the definition of steel self-centring moment resisting frames (SC-MRFs) have been proposed and developed over the past two decades. These usually consist of self-centring beam-to-column connections post-tensioned through high strength post-tensioned bars (PT-bars) or strands allowing a gap opening mechanism at the beam-to-column interface. The high strength PT bars provide restoring forces to return the structures in a plumb, whereas the dissipation of the seismic energy is provided by designed devices which are included in the self-centring connections (*e.g.*, [5]-[8]). Other recent research works have been devoted to the development of damage-free self-centring column bases (SC-CBs) (*e.g.*, [9]-[19]), based on the combination of rocking systems, dissipative devices and post-tensioned bars. Amongst others, Freddi *et al.* [15] presented and experimentally investigated [16] a rocking damage-free steel SC-CB equipped with friction devices (FDs) and high-strength steel PT bars. Kamperidis *et al.* [17] proposed a partial strength, low-damage, steel SC-CB equipped with PT tendons and hourglass shape steel yielding devices to dissipate the seismic energy. A similar approach was also followed by Wang *et al.* [18] while considering a concrete-filled square steel section as CB footing. Moreover, Latour *et al.* [19] developed and experimentally investigated a SC-CB consisting of a slotted column splice where the seismic behaviour is controlled by a combination of FDs, providing energy dissipation capacity, and PT bars with disk springs, introducing restoring forces in the connection. The overall connection has dimensions comparable to the size of a traditional column splice. It is located above a traditional full-strength base plate joint, as illustrated in Figure 1. The FDs are composed of friction pads coated with thermally sprayed metal, pre-stressed with high strength bolts, placed between the steel cover plates and the column. The disk springs, arranged in parallel and series, act as a

1. University of Salerno, Salerno, Italy.
2. University College London, London, UK.

macro-spring system, ensuring sufficient deformability to the connection and an adaptable stiffness resistance combination.

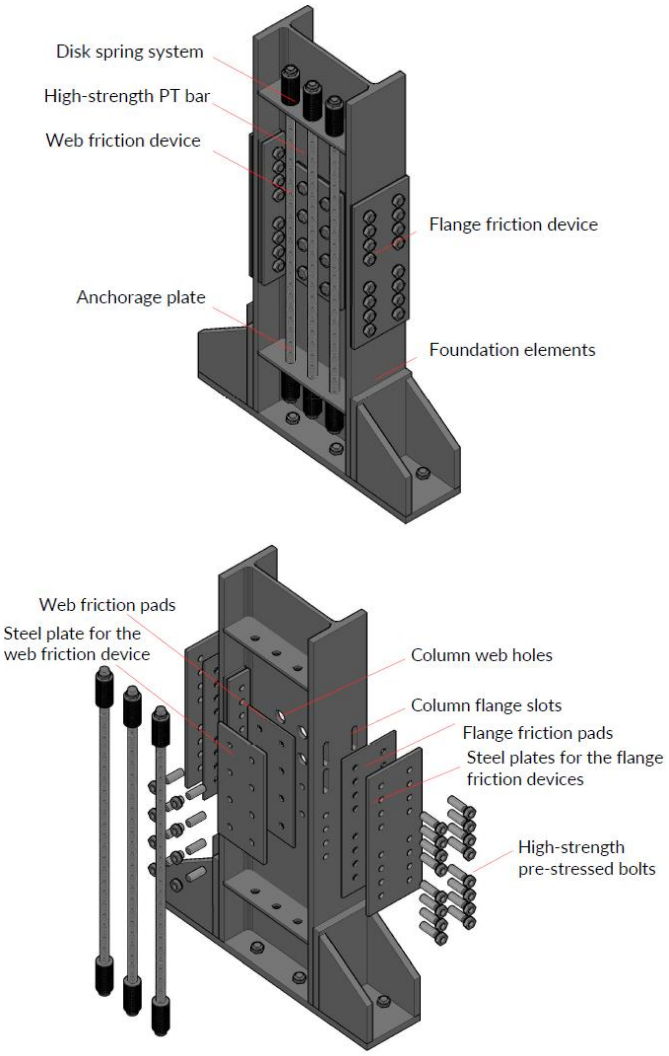

Figure 1 (a) 3D view; (b) 3D exploded view of the self-centring column base connection

Considering this connection typology, Elettore *et al.* [20] recently investigated, through numerical simulations, the seismic response of a 4-storey and 3-bay MRF, which uses conventional beam-to-column joints and the SC-CB connections developed by Latour *et al.* [19]. The results show that the introduction of SC-CBs is an effective strategy to reduce the residual drifts of the whole frame and protect the first storey columns from yielding, with the additional benefit of limiting the number of self-centring devices. Although several technologies for self-centring connections have been developed for both beam-to-column and CB joints, only a few research studies investigated the significant parameters (*e.g.*, properties of beam-to-column connections, properties of the CBs, frame layout) that influence the self-centring capability of these systems providing useful insights for the design. Moradi *et al.* [21] conducted a parametric analysis to study the influence of material and geometrical properties of PT beam-to-column connections (*i.e.*, beam depth, column height, and PT strand force) on the lateral response of these systems. Kamperidis *et al.* [22] investigated the effects of several specific local structural properties of the SC-CBs (*i.e.*, the initial stiffness, post-yield stiffness and strength of the CBs) on the seismic performance and collapse capacity of the benchmark frame. Moreover, Herning *et al.* [23] performed a reliability-based study to investigate the sensitivity of SC-MRFs performances to some structural properties and geometry (*i.e.*, PT beam-to-column connection details).

Within this context, the present paper performs a parametric analysis to investigate the frame layout's influence on the self-centring capability of perimeter MRFs with the SC-CB connections proposed in [19]. Nine case-studies buildings with a different number of storeys (*i.e.*, 4, 6 and 8) and bays (*i.e.*, 5, 7 and 9) have been designed according to the Eurocode 8 [1] and numerically investigated. State-of-the-art numerical models of the frames have been developed in OpenSees [24], with and without the investigated SC-CB connections. Incremental Dynamic Analyses (IDAs) [25] have been carried out considering a set of 30 ground motion records accounting for the influence of the uncertainty related to the earthquake input, *i.e.*, the record-to-record variability. The spectral acceleration corresponding to the fundamental period of vibration ($Sa(T_1,\xi)$) has been used as intensity measure (IM) while both global, and story-level engineering demand parameters (EDPs) have been monitored in order to compare the seismic performances of the frames. Fragility curves [26] have been successively developed, providing the probability of exceeding a residual interstorey drift limit equal to the 0.5%, conventionally associated with building reparability [4]. Results highlight that the efficiency of the SC-CBs in reducing the residual interstorey drifts is significantly affected by the number of storeys of the frames. In particular, the SC-CBs contributes to maximizing the self-centring capability at the lower storeys for all the structures, while its efficiency decreases along with the height.

2 Case-study frames

2.1 Design of the case-study frames

Nine case-studies buildings with a different number of storeys (*i.e.*, 4, 6 and 8) and bays (*i.e.*, 5, 7 and 10) have been designed according to the Eurocode 8 [1] to investigate the influence of the layout of the frame on the seismic performance of perimeter MRFs with SC-CBs. The plan and the elevation views of the case-study frames are shown in Figure 2(a) and (b), respectively. The nine case-study buildings have 4, 6 and 8 storeys; 5, 7 and 10 bays in the x-direction and 3 bays in the y-direction. The horizontal resisting system is composed by perimeter MRFs, while the interior part is composed of gravity frames (*i.e.*, with 'pinned' beam-to-column connections and 'pinned' CBs). The layout has interstorey heights of 3.20 m except for the first level, whose height is equal to 3.50 m, while all the bays, in both directions, have spans of 6 m. The study investigates the seismic response of the MRFs in the x-direction having 3, 5 and 8 bays. Two configurations are analysed and compared for each case-study: the first is the 'equivalent' MRF with conventional full-strength CBs, the second is the MRF including the SC-CB connections designed following the methodology presented in the next paragraph. The Type-1 elastic response spectrum with a 2% damping factor ξ, a peak ground acceleration (PGA) equal to 0.35g, and soil type C is considered for the definition of the Design-Based Earthquake (*i.e.*, DBE, Ultimate Limit State according to the European definition).The behaviour factor used for the definition of the design spectrum is equal to q = 6.5 in accordance with the requirements of the Eurocode 8 [1] for MRFs in DCH. The Maximum Credible Earthquake (*i.e.*, MCE, Collapse Limit State according to the European definition) is assumed to have an intensity equal to 150% the DBE.

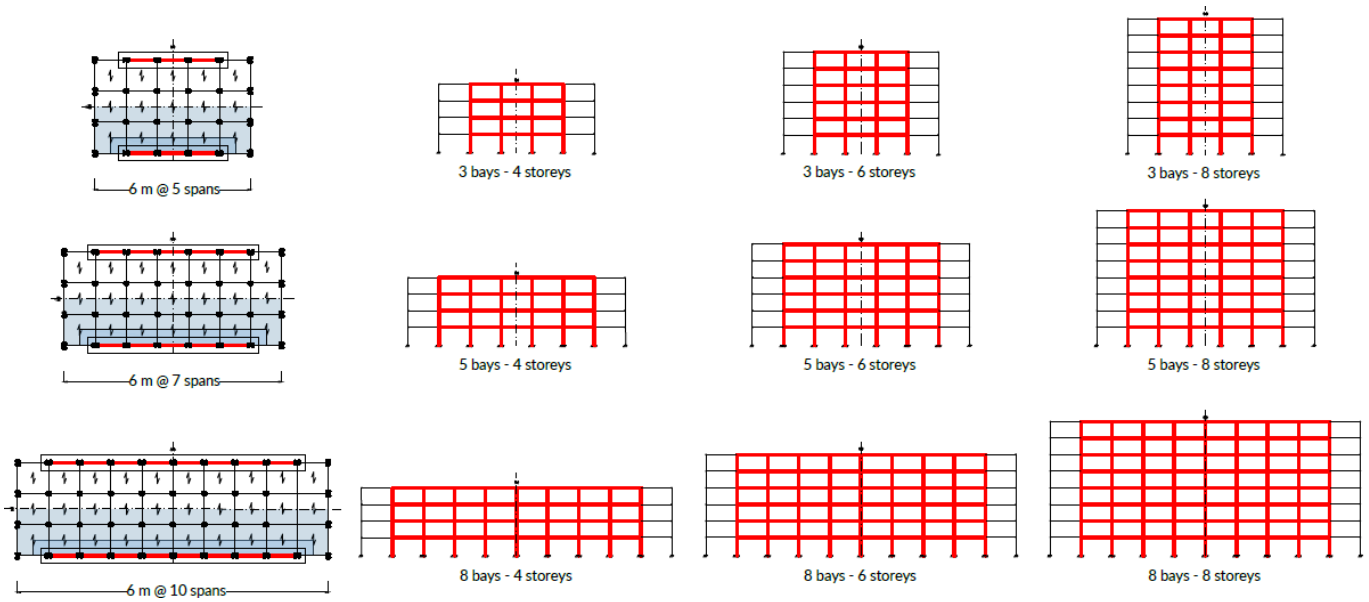

Figure 2 Case-study buildings: (a) Plan views; (b) Elevation views.

Steel S275 (yield stress f_y = 275 MPa) and S355 (f_y = 355 MPa) are used respectively for beams and columns. Beam-to-column connections are conventional full-strength rigid joints. The panel zones are stiffened with doubler plates with a thickness equal to the one of the column's web in order to ensure adequate strength to the joints hence promoting the plastic engagement of the beams only, in accordance with the capacity design rules. The floor is made by HI BOND A55/P600 type, hence ensuring the slab's rigid behaviour. The interstorey drift limit for the Damage State Limitation (DSL) requirements is assumed equal to 1% as suggested by Eurocode 8 [1] for structures having non-structural elements fixed in a way so as not to interfere with structural deformations. Table 1 reports the profiles' cross-section for each of the designed case-study frames, while Table 2 reports the fundamental periods of vibrations and the spectral accelerations corresponding to both the DBE ($S_{a,DBE}$) and MCE ($S_{a,MCE}$). The acronym MRF 3-4 indicates the case-study frame with 3-bays and 4-storeys and a similar abbreviation is used for the other case-study frames. The P-delta effects are not taken into account during the design since the interstorey drift sensitivity coefficient θ is less than 0.1, at all the storeys of all the case-study frames, where θ is calculated following Eurocode 8 requirements [1].

Table 1 Member cross-sections

Floor	Beams	Columns	Beams	Columns	Beams	Columns
	MRF 3-4		MRF 3-6		MRF 3-8	
1st	IPE 550	HE 550M	IPE 600	HE 600M	IPE 600	HE 650M
2nd	IPE 550	HE 550M	IPE 600	HE 600M	IPE 600	HE 650M
3rd	IPE 550	HE 450M	IPE 600	HE 500M	IPE 600	HE 600M
4th	IPE 550	HE 450M	IPE 600	HE 500M	IPE 600	HE 600M
5th			IPE 550	HE 400M	IPE 550	HE 600M
6th			IPE 550	HE 400M	IPE 550	HE 500M
7th					IPE 500	HE 500M
8th					IPE 500	HE 500M
	MRF 5-4		MRF 5-6		MRF 5-8	
1st	IPE 550	HE 450M	IPE 600	HE 500M	IPE 600	HE 650M
2nd	IPE 550	HE 450M	IPE 600	HE 500M	IPE 600	HE 650M
3rd	IPE 550	HE 360M	IPE 600	HE 400M	IPE 600	HE 600M
4th	IPE 550	HE 360M	IPE 600	HE 400M	IPE 600	HE 600M
5th			IPE 550	HE 340M	IPE 550	HE 600M
6th			IPE 550	HE 340M	IPE 550	HE 500M
7th					IPE 500	HE 500M
8th					IPE 500	HE 500M
	MRF 8-4		MRF 8-6		MRF 8-8	
1st	IPE 550	HE 450M	IPE 600	HE 450M	IPE 600	HE 600M
2nd	IPE 550	HE 450M	IPE 600	HE 450M	IPE 600	HE 600M
3rd	IPE 550	HE 360M	IPE 600	HE 360M	IPE 600	HE 550M
4th	IPE 550	HE 360M	IPE 600	HE 360M	IPE 600	HE 550M
5th			IPE 550	HE 320M	IPE 550	HE 550M
6th			IPE 550	HE 320M	IPE 550	HE 500M
7th					IPE 500	HE 500M
8th					IPE 500	HE 500M

Table 2 Fundamental Period (T1) and spectral acceleration (Sa(T1,ξ)) for DBE and MCE

Case-study	T_1 [sec]	$S_{a,DBE}$ [g]	$S_{a,MCE}$ [g]
MRF 3-4	0.70	1.02	1.54
MRF 3-6	0.96	0.75	1.12
MRF 3-8	1.27	0.57	0.85
MRF 5-4	0.72	1.00	1.50
MRF 5-6	0.97	0.74	1.12
MRF 5-8	1.17	0.61	0.92
MRF 8-4	0.69	1.05	1.57
MRF 8-6	0.96	0.75	1.13
MRF 8-8	1.15	0.63	0.94

2.2 Moment-rotation behaviour and design of the self-centring column base (SC-CB) connections

The column base connection experimentally tested by Latour *et al.* [19] and considered in this paper exhibits a moment rotation hysteretic behaviour which is function of the response of each component of the connection and can be represented by flag-shape curve. The expected forces of each component during the rocking behaviour are reported in

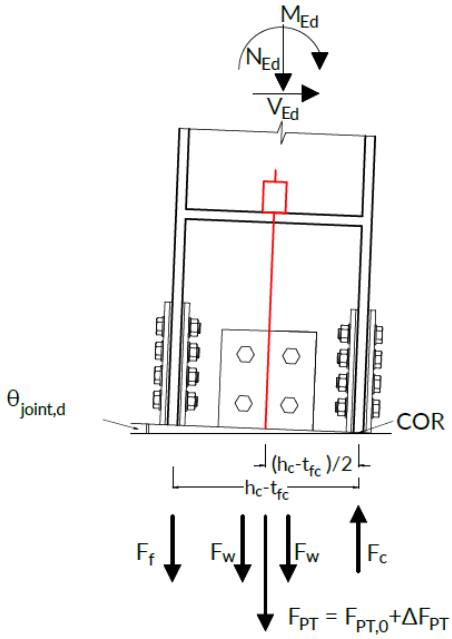

Figure 3(a). In this figure, F_C represents the compression force at the centre of rotation (COR); F_w and F_f represent the sliding forces in the friction pads on the column web and flanges respectively; F_{PT} is the sum of the initial post-tensioning forces $F_{PT,0}$, and the additional force consequent to the gap opening while rocking ΔF_{PT}. Additionally, N_{Ed}, M_{Ed} and V_{Ed} are the design actions (*i.e.*, axial force, bending moment and shear force) applied to the joint section, h_c is the height of the column section and t_{fc} is the thickness of the column flange. The flag-shape moment-rotation hysteretic loop is illustrated in

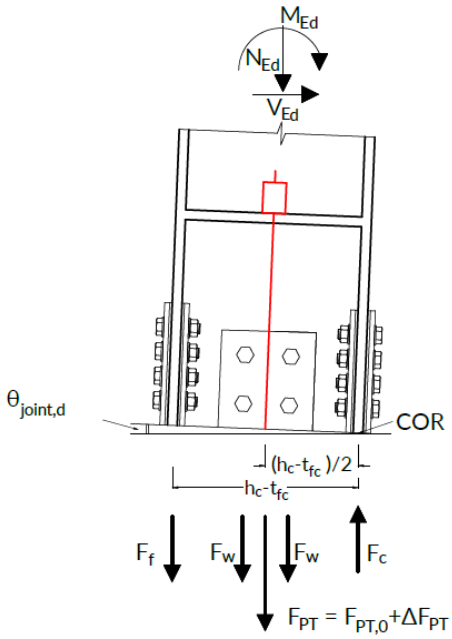

Figure 3(b) where: M_D is the decompression moment, *i.e.*, the sum of the moment contributions of the axial force M_N and the moment provided by the PT bars at zero rotation $M_{PT,0}$; M_{FD} is the moment provided by the FDs. M_1 is the moment that initiates the gap opening while M_2 is the maximum moment achieved at the design rotation $\theta_{joint,d}$ (*e.g.*, 0.04 rads as suggested by AISC 341-16 [3] for Special Moment Frames). The moments defining of the entire cyclic moment-rotation behaviour are given by:

$$\boldsymbol{M_D} = \left(\boldsymbol{N_{Ed}} + \boldsymbol{F_{PT,0}}\right)\left(\frac{\boldsymbol{h_c}-\boldsymbol{t_{fc}}}{2}\right) \quad (1)$$

$$\boldsymbol{M_{FD}} = \boldsymbol{F_f}\left(\boldsymbol{h_c}-\boldsymbol{t_{fc}}\right) + \boldsymbol{2F_w}\left(\frac{\boldsymbol{h_c}-\boldsymbol{t_{fc}}}{2}\right) \quad (2)$$

$$\boldsymbol{M_2} = \boldsymbol{M_D} + \boldsymbol{M_{FD}} + \boldsymbol{K_{eq}\theta_{joint}}\left(\frac{\boldsymbol{h_c}-\boldsymbol{t_{fc}}}{2}\right) \quad (3)$$

where K_{eq} is the equivalent axial stiffness of the system PT bars and disk springs [20] defined as follows:

$$\boldsymbol{K_{eq}} = \frac{\boldsymbol{K_{PT}K_{ds}}}{\boldsymbol{K_{PT}+K_{ds}}}; \quad \boldsymbol{K_{PT}} = \frac{\boldsymbol{n_{PT}E_{PT}A_{PT}}}{\boldsymbol{l_{PT}}}; \quad \boldsymbol{K_{ds}} = \frac{\boldsymbol{n_{ds,par}}}{\boldsymbol{n_{ds,ser}}}\boldsymbol{K_{ds,1}}; \quad (4)$$

.

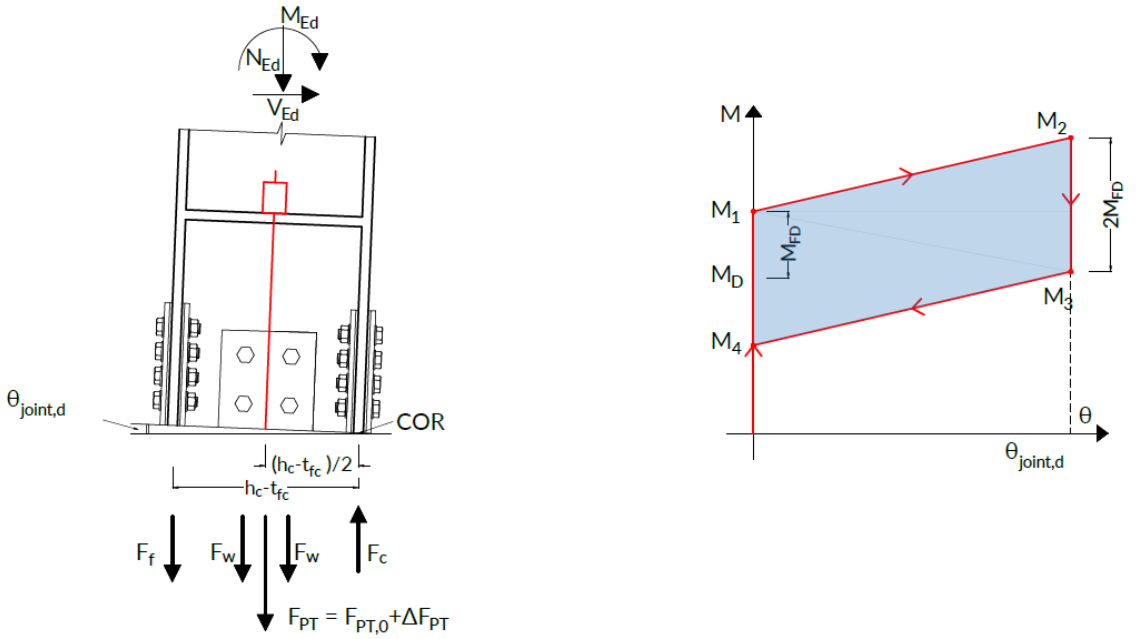

Figure 3 (a) Force interaction among the components during rocking; (b) Theoretical moment-rotation hysteretic curve.

The design of the proposed SC-CBs is based on the structural analysis of an 'equivalent' MRF with a fixed base. The axial design load N_{Ed} is derived from the amplified combination as required by Eurocode 8 [1], (*i.e.*, $N_{Ed} = N_{Ed,G} + 1.1\gamma_{ov}\Omega N_{Ed,E}$) The design moment M_{Ed} is calculated considering the amplified combination as required by Eurocode 8 [1], (*i.e.*, $M_{Ed} = M_{Ed,G} + 1.1\gamma_{ov}\Omega M_{Ed,E}$) while the design shear force is assumed equal to $V_{Ed} = M_{Ed}/L_0$, where L_0 is the shear length. Two main requirements must be satisfied during the design [20]: 1) the maximum moment of the SC-CB, M_2, is lower than the yielding moment of the column $M_{pl,c}$; 2) the self-centring behaviour of the connection is achieved if the decompression moment M_D, is higher than the moment contribution of the FDs, M_{FD}.

The friction pads are chosen according to the results of previous tests carried out by Cavallaro *et al.* [28] and consist of 8 mm of thermally sprayed friction metal steel shims with friction coefficient equal to $\mu = 0.53$. The bolts for the FDs of web and flanges are HV M30 10.9 class; the PT bars are high-strength M36 with a maximum post-tensioning capacity of 514 kN, while the resistance and the stiffness (K_{ds1}) of each disk spring are 200 kN and 100 kN/mm, respectively. The material properties are summarised in Table 3 where E, fy and f_u are the nominal values of the Young's modulus, the yield strength and ultimate tensile strength of the materials, respectively. The other properties of the adopted structural steel (*i.e.*, the shear modulus, the Poisson's ratio) are based on the Eurocode 3 [27]. Table 3 Material properties of the column base connections

Elements	Class [-]	E [GPa]	fy [Mpa]	fu [MPa]
Column and plates	S355	210	355	510
Post-tensioned bars	10.9	205	900	1000
Web bolts	10.9	210	900	1000
Flange bolts	10.9	210	900	1000

Table 4 summarises the number and the pre-load for the bolts of the FDs and PT bars of the inner and outer columns.

Table 3 Material properties of the column base connections

Elements	Class [-]	E [GPa]	f_y [Mpa]	f_u [MPa]
Column and plates	S355	210	355	510
Post-tensioned bars	10.9	205	900	1000
Web bolts	10.9	210	900	1000
Flange bolts	10.9	210	900	1000

Table 4 Components of the self-centring column base connections

Case-study	Number of PT Bars [-]	Number of Web bolts [-]	Pre-load web bolts [kN]	Number of Flange bolts [-]	Pre-load Flange bolts [kN]	Number of PT Bars [-]	Number of Web bolts [-]	Pre-load web bolts [kN]	Number of Flange bolts [-]	Pre-load Flange bolts [kN]
	Outer column					Inner column				
MRF 3-4	8	4	135	8	110	6	4	155	8	130
MRF 3-6	8	4	140	8	135	6	4	175	8	105
MRF 3-8	8	4	140	8	75	4	4	170	8	100
MRF 5-4	8	4	120	8	105	6	4	125	8	120
MRF 5-6	8	4	130	8	120	6	4	165	8	100
MRF 5-8	8	4	135	8	135	6	4	170	8	80
MRF 8-4	8	4	135	8	150	6	4	165	8	155
MRF 8-6	8	4	130	8	120	6	4	160	8	100
MRF 8-8	8	4	140	8	140	6	4	170	8	100

2.3 Frame and column base modelling

Two-dimensional finite element (FE) models of the frames with and without the SC-CB connection are developed in OpenSees [24] for all case-studies. The '*Steel01*' material [24] with 355 MPa and 275 MPa yield strengths and 0.2% post-yield stiffness ratio is used for columns and beams, respectively. Beams are modelled by a lumped plasticity approach where the plastic hinges are modelled as suggested by Lignos and Krawinkler [29]. Conversely, columns are modelled with a distributed plasticity approach with non-linear beam-column elements with four integration points. At beam-to-column connections, the '*Scissor*' model [30] simulates the panel zone stiffness and strength. Geometric non-linearities are considered in the elements of the MRF. In addition, a leaning column is included in the structural model to consider the P-Δ effects related to the gravity frames [31]. The rigid-floor diaphragm is modelled by assigning a high value to the axial stiffness to the beams. Gravity loads are applied on the beams by considering the seismic combination of the Eurocode 8 [1], while the masses are concentrated at the beam-to-column connections. Damping sources other than the hysteretic energy dissipation are modelled through Rayleigh damping where the values of the mass-related and stiffness-related damping coefficients are considered for a damping factor of 2% for the first two vibration modes.

The SC-CB connections are implemented by following the modelling strategy proposed by Elettore *et al.* [20]. The rocking interface's rigid elements are modelled with elastic elements [24] with very high flexural stiffness. These are connected to four non-linear springs represented by zero-length elements in parallel with gap elements simulating the bilinear hysteretic response of the FDs and the contact behaviour of the column interfaces FDs are modelled by the '*Steel01*' material [24] considering a very high initial stiffness and very low post-elastic stiffness, while the contacts elements are defined by the '*Elastic compression-no tension*' (ENT) material [24] with very high compression stiffness to model the contact behaviour. A central zero-length translational spring with bilinear elastic-plastic behaviour is used to model the system of PT bars and disk springs. The initial post-tensioning force of the PT bars is modelled by imposing an initial strain equal to $F_{PT}/A_{PT}E_{PT}$ by using the '*Initial strain material*'[24].

3 Performance-based assessment of the case-study frames

3.1 Ground motion selection

Incremental Dynamic Analyses (IDA) [25] have been carried out to investigate the seismic performances of the nine case-study frames in both configurations (*i.e.*, with and without the SC-CB connections). A suite of 30 ground motion records is selected from the SIMBAD Database using REXEL [32] accounting for the record-to-record variability. The set of ground motions is selected for each case-study with the following parameters: moment magnitude (M_w) ranging from 6 to 7, epicentral distance R ≤ 30 km and spectrum-compatibility in the range of periods between $0.2T_1$ and $2T_1$, where T_1 is the fundamental period of the structure. The mean elastic spectrum of the records is kept between 75% and 130% of the corresponding Eurocode 8 based elastic response spectrum [1] considered for the design. It is noteworthy that a large number of zero acceleration points (*i.e.*, 30 s) have been added at the end of each record to allow the free vibrations to stop and correctly capture the residual deformations.

Within the IDA procedure, the ground motion records are scaled to increasing IM values with a constant step of 0.1g until 'collapse'. The spectral acceleration corresponding to the first vibration mode ($Sa(T_1,\xi)$) is used as IM. It is important to highlight that the vibration periods, and consequently the IM values, are the same for the two 'equivalent' structures with and without the SC-CBs hence allowing the comparison of fragility curves

3.2 Incremental Dynamic Analysis

Global and storey-level EDPs are monitored to investigate the influence of the frame layout on the effectiveness of the proposed SC-CBs. Residual interstorey drifts are considered story-level EDPs, while the maximum values of these quantities among all the storeys are used as global EDPs. The effectiveness of the SC-CBs in reducing the residual interstorey drifts is evaluated by the comparison between 'equivalent' MRF with conventional full-strength CBs and the MRF with SC-CB connections (MRF-CB). In the present study, residual interstorey drifts limit is assumed equal to 0.5 %, which is the conventional threshold beyond which repairing may not be economically viable [4].

Figure 4 shows the comparison of the IDA results for all the considered structures (*i.e.*, with and without SC-CBs). The results are illustrated for the maximum (among all storeys) residual interstorey drifts ($\theta_{max\text{-}res}$). Red colour lines refer to IDA curves for the traditional MRF with conventional CBs (*i.e.*, MRF), whereas blue colour lines are related to the innovative configurations with SC-CBs (*i.e.*, MRF-CB). Highlighted in the figures are the 50% fractiles (*i.e.*, median value) among all ground motions as a synthesis of the demand values for both configurations. Additionally, the percentage reduction (Δ) of the aforementioned parameter is reported for the two seismic intensities of interest.

The figure highlights that the use of the SC-CBs allows for a significant residual drift reduction for all structures for both the DBE and the MCE. The only exception is related to the 8-storey frames where the percentage reduction is limited at the DBE (*i.e.*, from 0% to 13%). However, it is noteworthy that for all the structures equipped with the SC-CBs the median values of $\theta_{max\text{-}res}$ experience values lower than the limit of the 0.5%, also when the 'equivalent' conventional MRFs overcome it. The comparison of these reduction values provides an understanding of the frame layout's influence on the effectiveness of the proposed SC-CBs in terms of residual drifts reduction.

In particular, the results show a high sensitivity of the self-centring response to the number of storeys of the structures. This is evidenced by the percentage reductions Δ observed in Figure 4 (a), (b) and (c) of the 3-bay 4-storey, 3-bay 6-storey and 3-bay 8-storey frames, which assume decreasing values at the MCE (*i.e.*, from 70% to 36%). A similar trend can be seen for the 5-bay frames (*i.e.*, from 66% to 36%) and the 8-bays frames (*i.e.*, from 72% to 41%), at the same intensity, as shown in Figure 4 (d), (e) and (f) and Figure 4 (g), (h) and (i), respectively. It is highlighted that these results are particularly relevant at the MCE, due to the high plastic engagement of the plastic hinges of the structures. Conversely, with respect to the number of bays, the response of the frames does not show a clear tendency. In fact, it is not possible to observe a significant influence of the number of bays in reducing the efficiency of the SC-CBs, as evidenced in Figure 4 (a), (d) and (g) by the values of the percentage reductions Δ of the 3-bay 4-storey, 5-bay 4-storey and 8-bay 4-storey frames, which experience similar values at the MCE (*i.e.*, from 66% to 72%). Similarly, this also occurs for the 6-storey frames (*i.e.*, from 42% to 54%) and the 8-storey frames (*i.e.*, from 36% to 41%) at the same intensity, as shown in Figure 4 (b), (e) and (h) and Figure 2 (c), (f) and (i), respectively. Moreover, it is not possible to see a consistent trend at the DBE intensity.

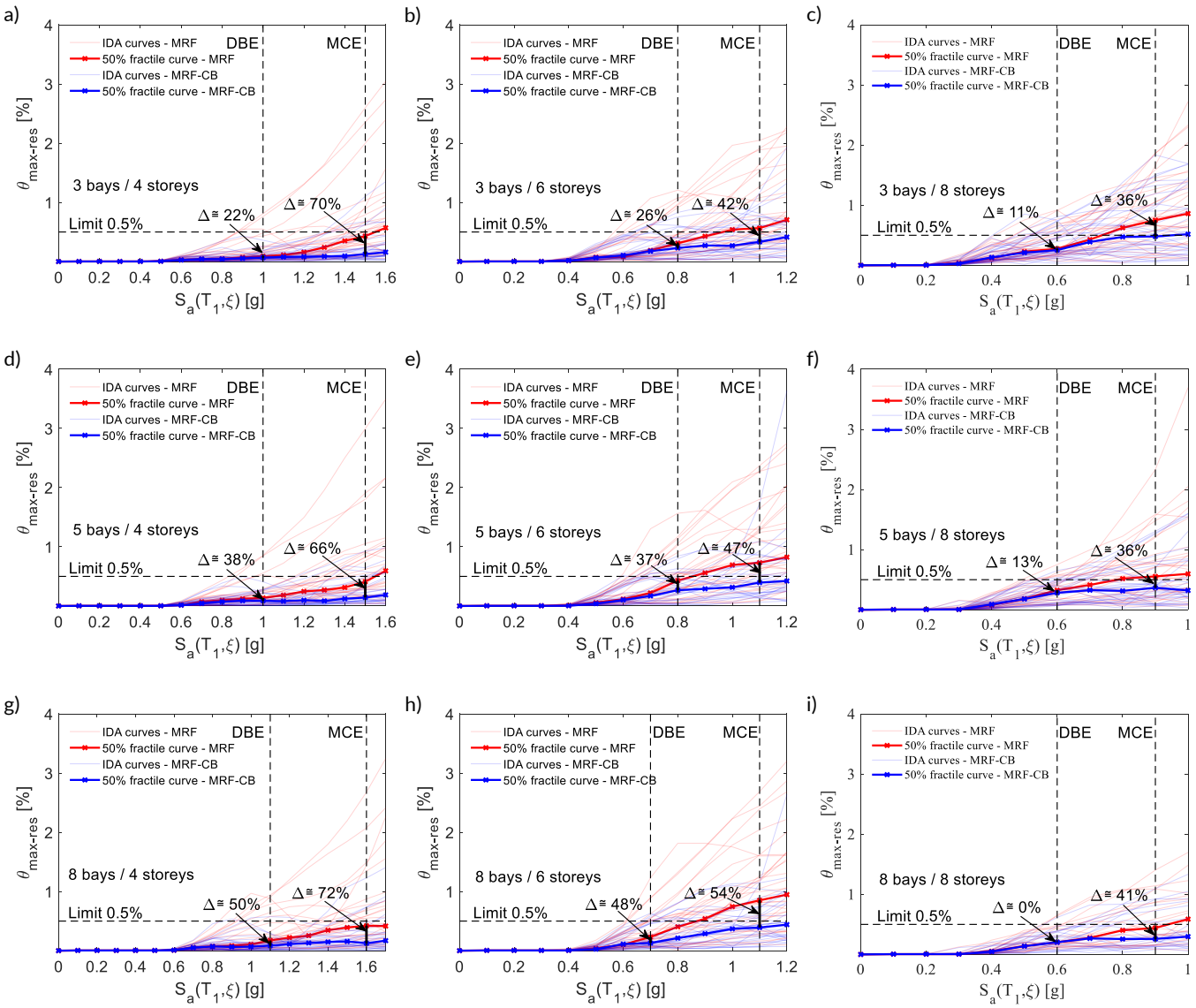

Figure 4 IDA Results. Comparison of the maximum interstorey drifts (a) 3-4; (b) 3-6; (c) 3-8; (d) 5-4; (e) 5-6; (f) 5-8; (g) 8-4; (h) 8-6; (i) 8-8

In order to provide additional information about the trends of the selected EDPs at all the storeys of the case-studies in both configurations, the height-wise residual interstorey drift distributions are shown in Figure 5. The figure shows the comparison of the residual interstorey drift distributions synthesized by the median value ($\theta_{res,50}$) for all the structures with and without the SC-CBs, at the MCE. For the structures with SC-CBs, a significant reduction of the residual interstorey drifts in the lower storeys can be observed, while its effectiveness reduces and tends to disappear at higher storeys. For example, for the 5-bay 6-storey frames the value of $\theta_{res,50\%}$ is reduced by 83% (*i.e.*, from 0.71% to 0.12%) at the first storey, by 55% (*i.e.*, from 0.55% to 0.25%) at the third storey and by 41% (*i.e.*, from 0.083% to 0.049%) at the sixth storey. Similar trends can be seen for the other case-studies.

It is worth mentioning that for the MRF with conventional CBs the maximum values of the residual interstorey drifts tend to concentrate at intermediate storeys for the 8-storey frames. This highlights the influence of the higher modes in the response of these structures. Conversely, for the 4- and 6-storey frames, $\theta_{res,50\%}$ assumes its maximum value at the lower storeys.

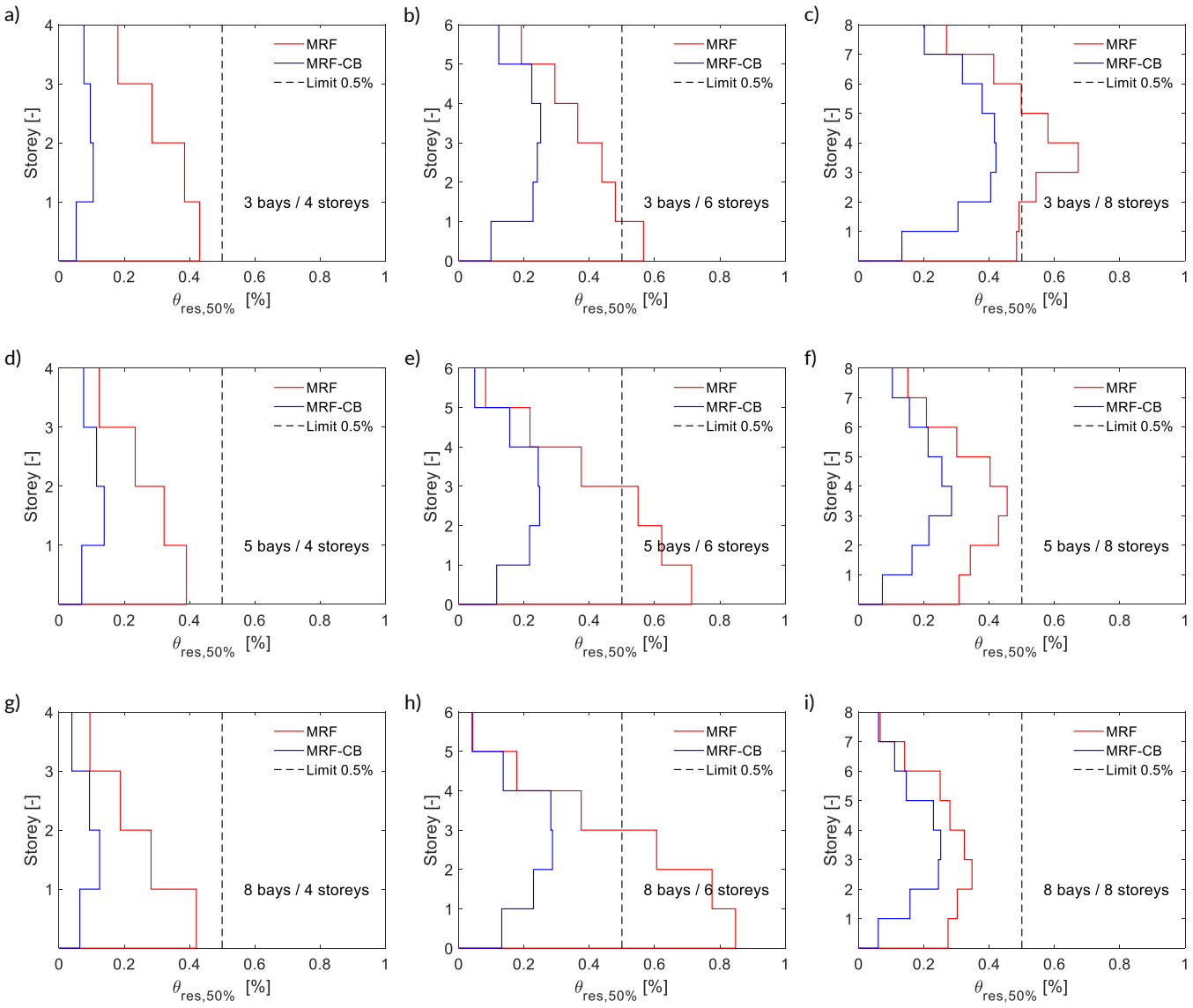

Figure 5 IDA Results: Comparison of the distribution of the residual storey drifts in terms of median values (50% fractile) among all ground motions of the case-study frames for MCE: (a) 3-4; (b) 3-6; (c) 3-8; (d) 5-4; (e) 5-6; (f) 5-8; (g) 8-4; (h) 8-6; (i) 8-8

3.3 Fragility curves

Fragility curves are used in order to quantify the probability of the seismic demand exceeding an associated capacity threshold, given the seismic intensity, which is characterized by the IMs [33]. In this study, the spectral acceleration corresponding to the first vibration period (*i.e.*, $Sa(T_1,\xi)$) is assumed as IM. Storey-level residual response parameters (*i.e.*, the storey-level residual interstorey drifts) are considered as EDPs. These values are compared with the associated capacity threshold which is conventionally assumed as 0.5% [4]. Numerical fragility curves are initially derived based on EDPs-IMs pairs obtained by the IDAs and successively fitted by analytical lognormal curves trough least-square minimization.

Such storey-level fragility curves provide the probability of exceeding the threshold limit of 0.5% (*i.e.*, probability of failure P_f) vs the seismic IM values, at each storey and for each case-study. Figure 6 shows the comparison of the storey-level fragility curves of all the case-study frames for the two configurations (*i.e.*, with and without the SC-CBs). The colour filled areas represent the interval between the most and the least fragile storeys (*i.e.*, red for the frames with conventional CBs, blue for the frames equipped with the SC-CBs). It is noteworthy that the fragilities provide a probabilistic interpretation of the results previously reported. In fact, in Figure 6 it is possible to observe a correlation with the height-wise distributions showed in Figure 5, in probabilistic terms. Figure 6 shows that, for all the structures equipped with conventional CBs, P_f is maximum at the 1st storey. The only exceptions are related to the 8-storey frames, where P_f is higher at the intermediate storeys (*i.e.*, 3rd – 4th storey), due to the influence of the higher modes. Conversely, P_f assumes the minimum values at the upper storeys. This behaviour highlights that the higher storeys of the structures experience smaller post-elastic deformations, as a consequence of the technological and design criteria adopted [1].

Regarding the structures equipped with the SC-CBs, the introduction of the proposed connections minimizes the probability of exceeding the 0.5% limit at the 1st storey (*i.e.*, $P_f \cong 0$). In some cases (*i.e.*, 8 bay 4 storey, 5 bay 6 storey and 8 bay 6 storey frames), due to the almost-elastic behaviour of the beams at the last storeys, the P_f of the last storeys assumes similar values to P_f at the 1st storey. Conversely, P_f is maximum at the intermediate storeys. These results demonstrate how the adoption of the SC-CBs provides a significant reduction of P_f at the lower storeys, while this effectiveness decreases along with the height, resulting in a reduction of the self-centring capability. To overcome this drawback, Pieroni *et al.* [34] is focusing on the investigation of optimum locations for damage-free self-centring devices in beam-to-column connections within mid-

rise frames, such that the self-centring capability is maximised also at the upper storeys.

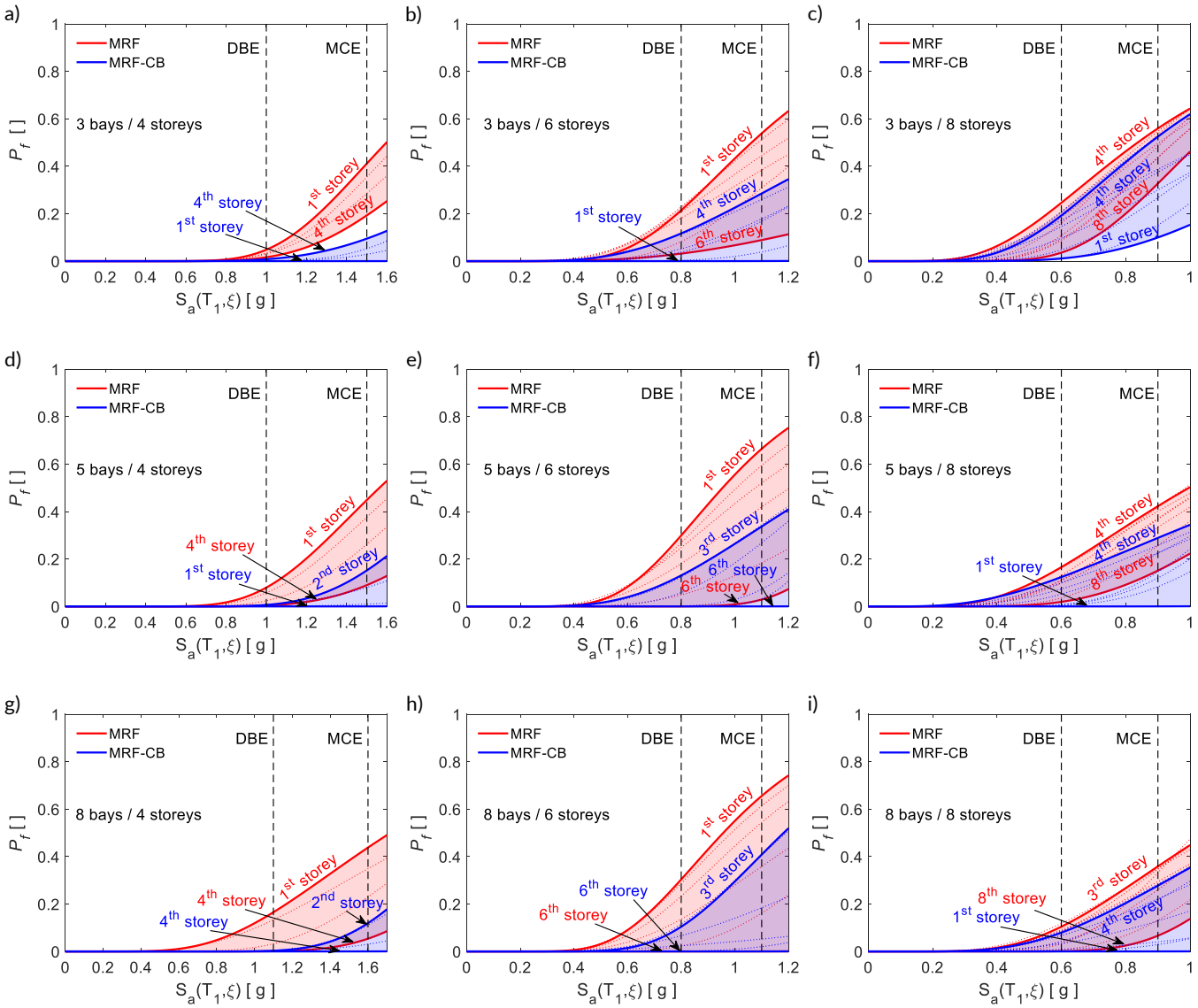

Figure 6 Comparison of the storey-level fragility curves for the residual interstorey drifts with respect to the threshold limit of 0.5%, for the case study frames: (a) 3-4; (b) 3-6; (c) 3-8; (d) 5-4; (e) 5-6; (f) 5-8; (g) 8-4; (h) 8-6; (i) 8-8.

4 Conclusions

This study performs a parametric analysis with the aim of investigating the influence of the frame layout on the self-centring capability of perimeter steel Moment Resisting Frames equipped with damage-free self-centring column base connections, previously proposed by the authors. Nine case-study frames with a different number of storeys (*i.e.*, 4, 6 and 8) and bays (*i.e.*, 3, 5 and 8) have been designed and numerically investigated in OpenSees. Each case-study is examined in two configurations (*i.e.*, with and without the damage-free self-centring column bases). Incremental Dynamic Analyses are performed with a set of 30 ground motion records, assessing both global and storey-level engineering demand parameter, while accounting for the record-to-record variability. Fragility curves are derived to evaluate the self-centring capability of the structures. The following conclusions can be drawn: 1) The seismic performances of the structures equipped with damage-free self-centring column base connections are significantly enhanced, as demonstrated by the significant residual drift reductions, at both the design based and maximum credible earthquake; 2) The self-centring capability of the adopted connections in reducing the residual interstorey drifts is particularly influenced by the number of storeys of the structures. Results show that the efficiency is relevant for the 4- and 6- storey frames, while it decreases for the 8-storey frames. Conversely, no sensitivity to the variation of the number of bays of the structures is observed; 4) The effectiveness of the adopted connection in reducing the residual interstorey drifts is relevant at the lower storeys, while it reduces at higher storeys, resulting in a reduction of the self-centring capability as evidenced by the 8- storey frames.

References

[1] EN 1998-1 (2004) *Eurocode 8: Design of structures for earthquake resistance – Part 1: General rules, seismic actions and rules for buildings*, European Committee for Standardization, Brussels.

[2] ASCE/SEI 7-16 (2017) *Minimum design loads and associated criteria for buildings and other structures*, American Society of Civil Engineers, Reston, USA.

[3] ANSI/AISC 341-16 (2016) *Seismic provisions for structural steel buildings*, American Institute of Steel Construction, Chicago, USA.

[4] McCormick, J., Aburano, H., Nakashima, M. (2008) *Permissible residual deformation levels for building structures considering both safety and human elements*, 14th World Conference on Earthquake Engineering (WCEE), October 12-17, Beijing, China.

[5] Ricles, J., Sause, R., Garlock, M., Zhao C. (2001) *Posttensioned Seismic-Resistant Connections for Steel Frames*, Journal of Structural Engineering; 127(2): 113–121.

[6] Christopoulos, C., Filiatrault, A., Uang, C-M., Folz, B. (2002) *Posttensioned energy dissipating connections for moment-resisting steel frames*, Journal of Structural Engineering; 128(9): 1111–20.

[7] Kim, HJ., Christopoulos, C. (2008) *Friction damped posttensioned self-centering steel moment-resisting frames*, Journal of Structural Engineering; 134(11): 1768–79.

[8] Vasdravellis, G., Karavasilis, TL., Uy, B. (2012) *Large-scale experimental validation of steel posttensioned connections with web hourglass pins*, Journal of Structural Engineering; 139: 1033–1042.

[9] Takamatsu, T., Tamai, H. (2005) *Non-slip-type restoring force characteristics of an exposed-type CB*, Journal of Constructional Steel Research; **61**(7): 942–961.

[10] Ikenaga, M., Nagae, T., Nakashima, M., Suita, K. (2006) *Development of CBs having self-centering and damping capability*. 5th International Conference on Behaviour of Steel Structures in Seismic Areas, Yokohama, Japan.

[11] Mackinven, H., MacRae, GA., Pampanin, S., Clifton, GC., Butterworth, J. (2007) *Generation four steel moment frame joints*. 8th Pacific Conference on Earthquake Engineering, Singapore.

[12] Chou, CC., Chen, JH. (2011) *Analytical model validation and influence of CBs for seismic responses of steel post-tensioned self-centering MRF systems*, Engineering Structures; **33**(9): 2628–2643.

[13] Chi, H., Liu, J. (2012) *Seismic behaviour of post-tensioned CB for steel self-centering moment resisting frame*, Journal of Constructional Steel Research; **78**: 117–130.

[14] Yamanishi, T., Kasai, K., Takamatsu, T., Tamai, H. (2012) *Innovative column-base details capable of tuning rigidity and strength for low to medium-rise steel structures*. 15th World Conference on Earthquake Engineering, Lisbon, Portugal.

[15] Freddi, F., Dimopoulos, CA., Karavasilis, TL. (2017) *Rocking damage-free steel CB with Friction Devices: design procedure and numerical evaluation*, Earthquake Engineering and Structural Dynamics; **46**: 2281–2300.

[16] Freddi, F., Dimopoulos, CA., Karavasilis, TL. (2020) *Experimental evaluation of a rocking damage-free steel CB with friction devices*, Journal of Structural Engineering. (ASCE); **146**(10): 04020217. DOI: 10.1061/(ASCE)ST.1943-541X.0002779.

[17] Kamperidis, V., Karavasilis, TL., Vasdravellis, G. (2018) *Self-centering steel CB with metallic energy dissipation devices*, Journal of Constructional Steel Research; **149**: 14–30.

[18] Wang, XT., Xie, CD., Lin, LH., Li, J. (2019) *Seismic behaviour of self-centering concrete-filled square steel tubular (CFST) CB*. Journal of Constructional Steel Research; **156**: 75–85.

[19] Latour, M., Rizzano, G., Santiago, A., Da Silva, L. (2019) *Experimental response of a low-yielding, self-centering, rocking CB joint with friction dampers*, Soil Dynamics and Earthquake Engineering; **116**: 580–592.

[20] Elettore, E., Freddi, F., Latour, M., Rizzano, G. (2020) *Design and analysis of a seismic resilient steel moment resisting frame equipped with damage free self-centring column bases*, Journal of Constructional Steel Research.

[21] Moradi, S., Alam, MS., (2017) *Lateral Load–Drift Response and Limit States of Posttensioned Steel Beam-Column Connections: Parametric Study*, Journal of Structural Engineering, 143(7): 04017044.

[22] Kamperidis, VC., Papavasileiou, GS., Kamaris, GS., Vasdravellis, G. (2020) *Seismic collapse of self-centering steel MRFs with different column base structural properties*, Journal of Constructional Steel Research; 175: 106364.

[23] Herning, G., Garlock, MEM., Vanmarcke, E. (2011) *Reliability-based evaluation of design and performance of steel selfcentring moment frames*, Journal of Constructional Steel Research; 67: 1495–1505.

[24] Mazzoni, S., McKenna, F., Scott, MH., Fenves, GL. (2009) *OpenSEES: Open System for earthquake engineering simulation*, Pacific Earthquake Engineering Research Centre (PEER), University of California, Berkley, CA, Available at: http://opensees.berkeley.edu.

[25] Vamvatsikos, D., Cornell, CA. (2002) *Incremental Dynamic Analysis*, Earthquake Engineering and Structural Dynamics; 31(3): 491–514.

[26] Shinozuka, M., Feng, MQ., Kim, H-K., Kim, S-H. (2000) *Non-linear static procedure for fragility curve development*, Journal of Engineering Mechanics; 126(12): 1287–95.

[27] EN 1993-1-8 (2005), *Eurocode 3: Design of steel structures, Part 1-8: Design of steel structure: General rules and rules for buildings*, European Committee for Standardization, Brussels.

[28] Cavallaro, GF., Francavilla, A., Latour, M., Piluso, V., Rizzano, G. (2008) *Cyclic behaviour of friction materials for low yielding connections*. Soil Dynamics and Earthquake Engineering; 114: 404–423.

[29] Lignos, D., Krawinkler, H., (2011) *Deterioration Modelling of Steel Components in Support of Collapse Prediction of Steel Moment Frames under Earthquake loading*, Journal of Structural Engineering; 137: 1291–1302.

[30] Charney, F., Downs, W., (2004) *Modelling procedures for panel zone deformations in moment resisting frames*. Connections in Steel Structures; ESSC/AISC Workshop, Amsterdam.

[31] Foutch, DA., Yun, S-Y., (2002) *Modeling of steel moment frames for seismic loads*, Journal of Constructional Steel Research; 58: 529–564.

[32] Iervolino, I., Galasso, C., Cosenza, E. (2010) *REXEL: Computer aided record selection for code-based seismic structural analysis*, Bulletin of Earthquake. Engineering; 8: 339–362.

[33] Cornell, CA., Jalayer, F., Hamburger, RO., Foutch, DA. (2002) *Probabilistic Basis for 2000 SAC Federal Emergency Management*

Agency Steel Moment Frame Guidelines. Journal of Structural Engineering; 128:526-533.

[34] Pieroni, L., Elettore, E., Freddi, F., Latour, M. (2021) *Optimized strategies for mid-rise seismic-resilient self-centring steel moment resisting frames.* The 9th European Conference on Steel and Composite Structures (Eurosteel 2020), Sheffield, UK, 1–3 September 2021.